Pergamon

Acta mater. Vol. 45, No. 8, pp. 3191–3202, 1997

Printed in Great Britain
PII: S1359-6454(97)00002-5
1359-6454/97 $17.00 + 0.00

SOLUTE-ATOM SEGREGATION TO ⟨110⟩ SYMMETRIC TILT GRAIN BOUNDARIES

J. D. RITTNER and D. N. SEIDMAN

Department of Materials Science and Engineering and the Materials Research Center, Northwestern University, 2225 N. Campus Dr., Evanston, IL 60208, U.S.A.

(Received 5 August 1996; accepted 17 December 1996)

Abstract—Segregation of substitutional, oversized solute atoms to both equilibrium and metastable structures of twenty-one ⟨110⟩ symmetric tilt grain boundaries (GBs) in an f.c.c. binary alloy is investigated with atomistic simulations. The Monte Carlo technique is employed to determine the interfacial excess and the solute distribution in GB structures for a bulk solute concentration of 4 at.%. Results from these simulations are used to demonstrate the shortcomings of simple geometric GB parameters for predicting variations in the interfacial excess from GB to GB. The interfacial excess is also found to vary from one structure to another for the same GB. An example of a segregation-induced congruent GB phase transition is also presented. Accurate segregation free energies for individual sites in GBs are calculated with the overlapping distributions Monte Carlo technique. Segregation entropies are determined and are found to be a linear function of the segregation internal energies for the same GB sites. © *1997 Acta Metallurgica Inc.*

1. INTRODUCTION

Segregation to grain boundaries (GBs) has been of interest since the 1930s when it was realized that some steels were susceptible to failure by intergranular fracture when certain impurities were present [1]. Segregation of impurities or intentionally added alloying elements at GBs can greatly affect various GB properties, which in turn affect numerous macroscopic material properties. Materials phenomena that have been linked to GB segregation include temper brittleness, fatigue strength, adhesion, precipitation, diffusional creep, intergranular corrosion, and GB diffusivity [1]. Although GB segregation has been extensively studied for many years [2], the effect of different GB structures on segregation was generally not considered. It has been established, both experimentally [3, 4] and theoretically [4, 5], that the level of segregation varies from GB to GB in the same alloy, but there is little direct information on how the GB structure influences segregation. Since segregation may also change the GB structure, structure and segregation are intimately connected.

In a recent paper [6] a thorough investigation was made of the structures of ⟨110⟩ symmetric tilt GBs in a low stacking-fault energy f.c.c. metal. A total of 21 different GBs with tilt angles between 0° and 180° were simulated with the molecular statics and Monte Carlo (MC) techniques. In many cases multiple GB structures were found. The stability of these structures at a temperature of 800 K was also tested. A number of novel GB structures were found in these simulations. One set of structures was used to develop a model for GB dissociation by stacking fault emission [7] that can be used to explain several recently observed experimental GB structures. In this paper we report on an investigation of substitutional solute-atom segregation to these GB structures. Equilibrium segregation is simulated with the MC technique using the transmutational ensemble. The interfacial excess of solute is calculated for each structure, in addition to the average solute concentration at individual sites in the structures. Structural changes resulting from segregation are also analyzed. Finally, a variation on the standard MC technique, called the overlapping distributions MC (ODMC) technique, is used to calculate segregation free energies at individual sites in GBs.

There are five macroscopic geometric degrees of freedom (DOF) required to specify a particular GB. These five DOF can be defined as the rotation axis, $\hat{\mathbf{c}}$, the rotation angle, θ, and the boundary plane unit normal, $\hat{\mathbf{n}}$. A single GB can have multiple structures that are characterized by different microscopic rigid-body translation (RBT) vectors and individual atomic relaxations. The five macroscopic DOF have been shown to be state variables for GBs along with the temperature, pressure and composition [8]. In true equilibrium the microscopic DOF are not state variables. For non-equilibrium situations, however, which may result from many processing techniques or internal constraints on a GB, the RBT vectors and atomic relaxations can be important for determining GB properties such as GB segregation.

The proper thermodynamic measure of segregation is the Gibbsian interfacial excess of solute, Γ_{solute} [9]. The interfacial excess is the amount of solute present

per unit area of interface in excess of the amount of solute that would be present if there were no interface. For a homophase GB the interfacial excess may be defined as

$$\Gamma_{\text{solute}} = \frac{N_{\text{excess}}}{A} = \frac{1}{A}\left(N_{\text{total}} - C_{\text{bulk}} V_{\text{total}}\right) \qquad (1)$$

where V_{total} is the volume of analysis, A is the interface area in this volume, N_{total} is the total number of solute atoms in V_{total}, and C_{bulk} is the bulk concentration of solute. The interfacial excess is often given in terms of monolayers of solute [10]. This unit of measure, however, requires knowledge of the planar density of atomic sites in a bulk plane parallel to the boundary. Also, the monolayer notation carries with it the implication that segregation occurs only in a single layer at the boundary. To avoid these problems, normalized units of atoms/nm^2 are employed.

The following section contains a brief overview of the two main simulation techniques and the interatomic potentials that are utilized. Results from the simulations on segregation to multiple structures, solute distributions, segregation-induced structural changes, and segregation free energies are presented and discussed in the third section. Finally, in the last section the main conclusions are summarized.

2. PROCEDURE

2.1. Monte Carlo simulations in the transmutational ensemble

To study equilibrium GB segregation at elevated temperatures, MC simulations with the transmutational ensemble are employed. This methodology has been used extensively to investigate both surface [11] and GB [4, 5, 12] segregation. During a simulation, the temperature, the total number of atoms, and the difference in the excess chemical potentials are held constant. The total volume of a computational cell is allowed to relax, i.e. expand or contract, with the net effect being a constant zero pressure. This volume relaxation allows for both thermal expansion of the bicrystal and an excess volume at the GBs. The chemical identities of atoms are changed randomly and the positions of the atoms are simultaneously relaxed. The chemical composition in the bulk volume regions is constant, due to the constant excess chemical potential difference. In the GB region the composition changes until the excess chemical potential difference is in equilibrium with the bulk regions, thereby producing solute-atom segregation. The sampling for both the changes in chemical identity and relaxation of the atomic positions is performed with the Metropolis algorithm [13].

The initial configurations are based on the pure Ni structures from Ref. [6] that remained stable during MC annealing simulations at 800 K. These bicrystals contain 6336–10,640 atoms. They are modified by randomly replacing 4% of the Ni atoms in the cells with Pd atoms. The volume of the cells is also scaled so that the bulk crystal regions have the correct equilibrium lattice constant for a Ni–4 at.% Pd alloy at 800 K. Three-dimensional Born–von Karman periodic border conditions are employed to eliminate surface effects. The periodic borders generate a second GB with the same misorientation and boundary plane at the sides of the computational cell normal to the boundary planes. The separation between the two GBs is sufficient to provide a bulk volume region of unstressed perfect crystal in the middle of each grain. The periodic borders perpendicular to the boundary plane are kept immobile to counteract the interfacial free energy of the GB and maintain the correct equilibrium lattice constant in the bulk volume regions. This procedure has been shown [14] to yield results equivalent to using mobile borders and much larger bulk volume regions that require significantly longer computational times.

2.2. Overlapping distributions Monte Carlo method

To calculate segregation free energies ΔF^{seg} the overlapping distributions Monte Carlo (ODMC) methodology [15] is employed. The segregation free energy is defined as the change in the free energy of the system when a solute atom moves from a bulk crystal region to the boundary. A positive ΔF^{seg} implies that the solute concentration is enhanced at the GB while a negative value indicates solute depletion. Although it is not possible to calculate directly free energies with MC simulations, the ODMC technique allows for the calculation of free energy differences such as ΔF^{seg}. The formulation of this methodology starts from the definition of the Helmholtz free energy from statistical mechanics:

$$F = -kT \ln(Z). \qquad (2)$$

The classical partition function Z is given by

$$Z = \int e^{-H/kT}\, d\mathbf{p}\, d\mathbf{q} \qquad (3)$$

where H is the Hamiltonian, $\mathbf{p}$ and $\mathbf{q}$ are the momentum and position vectors for the N atoms in the ensemble, and kT has its usual significance. If all the N atoms are of the same type, Z can be expressed as

$$\begin{aligned} Z &= \left(\int e^{-\mathbf{p}^2/2mkT}\, d\mathbf{p}\right)^N \int e^{-E/kT}\, d\mathbf{q} \\ &= (2\pi mkT)^{3N/2} \int e^{-E/kT}\, d\mathbf{q}. \end{aligned} \qquad (4)$$

The free energy difference ΔF between two arbitrary ensembles is

$$\Delta F = F_2 - F_1 = -kT \ln\left(\frac{Z_2}{Z_1}\right) \qquad (5)$$

where Z_1 and Z_2 are the partition functions of the two ensembles. To calculate ΔF^{seg} the first ensemble contains only solvent atoms and the second ensemble is identical except for the substitution of a single solute atom. With this choice of ensembles, the ratio

Z_2/Z_1 can be expressed in the form of a thermodynamic average over the first ensemble:

$$\frac{Z_2}{Z_1} = \left(\frac{m_2}{m_1}\right)^{3/2} \langle e^{-(E_2 - E_1)/kT} \rangle_1. \quad (6)$$

An MC simulation is used to sample this function over the first ensemble and calculate ΔF^{seg} at individual sites in a GB. The segregation free energy is calculated for a bulk concentration at the dilute limit since only one solute atom is present in the computational cell at a time. This approach has been used to study both surface and GB segregation [16, 17].

2.3. *Interatomic potentials*

The atomic interactions are calculated with the "universal" embedded atom method (EAM) potentials [18] for the Ni solvent and Pd solute atoms. Although problems have been reported for the Ni(Cu) alloy system with the universal EAM potentials [19], the experimental dilute heat of solution for the Ni(Pd) alloy system is well reproduced [18]. The EAM potentials are, however, known to underestimate stacking-fault energies. Thus, the pure Ni structures that serve as the starting configurations for the segregation simulations are interpreted as typical GB structures for f.c.c. metals with low stacking-fault energies. Palladium is chosen as the solute species because it is expected to segregate strongly in Ni, primarily due to its 10% size misfit. The ratio of the inhomogeneity factor to the size misfit factor (ϵ_K/ϵ_a) is less than unity for Ni(Pd), indicating that the elastic interaction between solute atoms and GBs in this system is dominated by the size misfit effect [20]. Also, since Ni and Pd have the same number of valence electrons, similar electronegativities, and complete solid solubility across the phase diagram, the electronic interaction is expected to be small.

3. RESULTS AND DISCUSSION

3.1. *Interfacial excess of solute*

Due to the difficulty of measuring GB segregation there have been many attempts to correlate the level of segregation at a GB with its geometry or crystallography. In general, Γ_{solute} is a function of the five macroscopic DOF of a GB [8]. This phase space is too large, however, to be of any practical use for predicting GB segregation behavior. It has been frequently suggested that with the proper transformation of variables, Γ_{solute} may depend primarily on a single parameter that is some function of the original five DOF. Some of the parameters that have been utilized include: (1) the inverse coincident site lattice density, (2) the GB planar coincident site density, (3) the GB average interplanar spacing, (4) the classification level, and (5) individual macroscopic DOF. Some examples where these geometric parameters have been correlated with Γ_{solute} values are presented below. The lowest Γ_{Pd} values for the 23 $\langle 110 \rangle$ tilt GBs in the Ni–4 at.% Pd system at 800 K are also plotted against these parameters to test for correlations. Limitations and problems with these geometric parameters are discussed.

One geometric parameter that is often used to predict segregation behavior is the inverse coincidence site density Σ. As early as 1959 [21], it was suggested that GBs with low values of Σ would have lower levels of segregation. It was observed that "special" GBs with a high degree of coincidence sites (low Σ) in lead migrated faster than general GBs when a small amount of tin was added. This was interpreted as indicating that the tin segregates more strongly to high Σ GBs [22]. One problem with Σ is that it is a function of only the misorientation between two crystals and the dependence on the interface plane is ignored. Thus, symmetric and asymmetric tilt GBs, twist GBs, and mixed twist–tilt GBs with the same value of Σ are all predicted to have the same Γ_{solute}. However, in a comparison of symmetric tilt GBs and twist GBs with the same Σ value, large differences in Γ_{solute} were observed [17]. Even if this criterion is applied only to sets of similar GBs, such as $\langle 110 \rangle$ symmetric tilt GBs, the correlation is still not very good. The lowest value of Γ_{Pd} found for each of the 23 $\langle 110 \rangle$ tilt GBs investigated in this paper is plotted against Σ in Fig. 1. There is no obvious correlation between Γ_{Pd} and Σ for these GBs. The highest value of Γ_{Pd} is found at a low $\Sigma = 9$ GB and one of the lowest values of Γ_{Pd} is found for a $\Sigma = 43$ GB.

Since Σ describes the three-dimensional coincidence site density for two crystals, a better parameter might be the two-dimensional planar coincident site density in the boundary plane. For symmetric tilt GBs this is proportional to another parameter, the average interplanar spacing parallel to the boundary. The average interplanar spacing d can be normalized by the lattice constant a_o to obtain a dimensionless parameter. Unlike the planar coincidence site density, the d/a_o parameter is not useful for describing twist GBs since the average interplanar spacing is

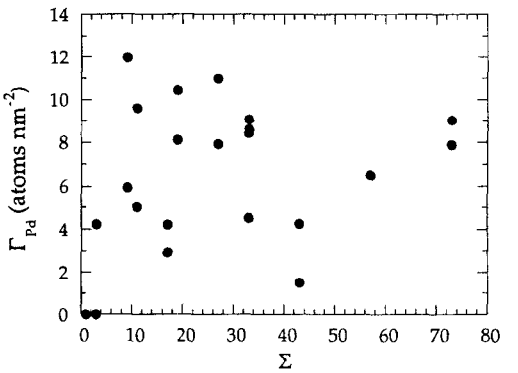

Fig. 1. The lowest interfacial excess of Pd vs the inverse coincident site lattice density (Σ) for the 23 $\langle 110 \rangle$ symmetric tilt GBs in Ni–4 at.% Pd at 800 K.

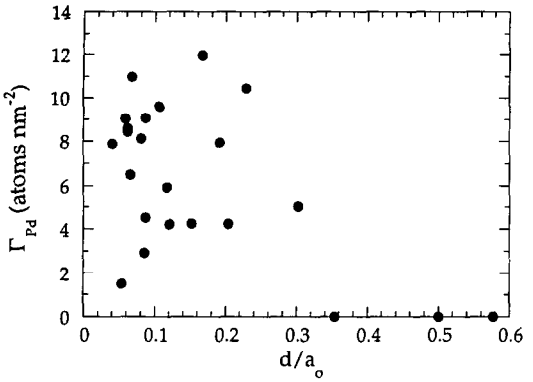

Fig. 2. The lowest interfacial excess of Pd vs the normalized interplanar spacing (d/a_o) for the 23 ⟨110⟩ symmetric tilt GBs in Ni–4 at.% Pd at 800 K.

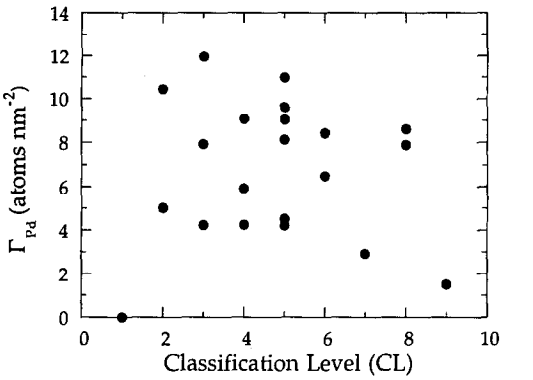

Fig. 3. The lowest interfacial excess of Pd vs the classification level (CL) for the 23 ⟨110⟩ symmetric tilt GBs in Ni–4 at.% Pd at 800 K.

independent of the twist angle, but it is useful for asymmetric as well as symmetric tilt GBs. It has been suggested [23] that GBs with a low planar coincident site density or d/a_o should have a higher level of segregation. Segregation energies ΔE^{seg} for C, P, and Si measured employing Auger electron spectroscopy (AES) at tilt GBs in Fe–3.5 at.% Si [24] were found to be high for GBs with $d/a_o < 0.2$ [25]. The lowest value of Γ_{Pd} found for each of the 23 ⟨110⟩ tilt GBs investigated in this research is plotted against d/a_o in Fig. 2. Although the three highest values of d/a_o—for the $\Sigma = 3/(111)/109.47°$ coherent twin GB, and the $\Sigma = 1/(001)/0°$ and $\Sigma = 1/(110)/180°$ perfect crystal orientations—had the lowest (or zero) values of Γ_{Pd}, there is no correlation for lower values of d/a_o. In fact, a GB with one of the lowest d/a_o values had the second lowest value of Γ_{Pd}.

The classification level (CL) [26] has also been suggested to correlate with Γ_{solute} [25]. Grain boundaries can be divided into different CLs with a formula that is based on the way d/a_o changes with the misorientation. A limitation of the CL is that it has been defined only for symmetric tilt GBs. For the tilt GBs in Fe–3.5 at.% Si, the ΔE^{seg} values for C, P, and Si were found to be low for GBs with CLs $\leqslant 3$, while they were higher for CLs $\geqslant 4$ [25]. The lowest value of Γ_{Pd} found for each of the 23 ⟨110⟩ tilt GBs investigated in this research is plotted against its CL in Fig. 3. Although Γ_{Pd} is very low for CL = 1, at higher CLs there is no correlation. The GB with the highest CL actually has the second lowest value of Γ_{Pd}.

Perhaps the most obvious choice for a parameter that might correlate with Γ_{solute} is just one of the original macroscopic DOF. For example, in many twist GBs Γ_{solute} is found to increase smoothly with the twist angle, θ, until it reaches a saturation level [14, 27]. In an experimental study using atom-probe field-ion microscopy (APFIM), rhenium segregation to ⟨110⟩ twist GBs in W–25 at.% Re was measured. Except for a large cusp at the $\Sigma = 3/(011)/70.53°$ GB, the Re enrichment factor increased smoothly with θ [28]. In another APFIM study, Γ_{Si} at GBs in Fe–3 at.% Si was measured [29]. The interfacial excess was found to be low for a small misorientation angle and higher at larger angles, but no strong correlation was observed. For the GBs in this study, θ was not the only macroscopic DOF that was varying, however. This illustrates the problem with correlating Γ_{solute} with only one macroscopic DOF when the other DOFs are not constant. This can even be a problem when there is only one independent DOF, such as for the ⟨110⟩ symmetric tilt GBs. For this set of GBs, the plane normal is not constant but is a function of θ. As a result, the dependence of Γ_{solute} on θ for tilt GBs is generally more complicated than it is for twist GBs. In Fig. 4 the Γ_{Pd} for each of the ⟨110⟩ tilt GB structures is plotted against the tilt angle θ. From the curve drawn through the lowest Γ_{Pd} for each GB it is clear that Γ_{Pd} is a function of θ but the relationship is complex. Since the curve is not very smooth, a large number of points are required to predict how Γ_{Pd} varies with θ.

While it is well known that Γ_{solute} often varies from GB to GB, the effect of multiple structures for a single GB on Γ_{solute} has generally not been considered. In Ref. [6] it is shown that many non-equilibrium structures are very stable, even at 800 K, in the pure

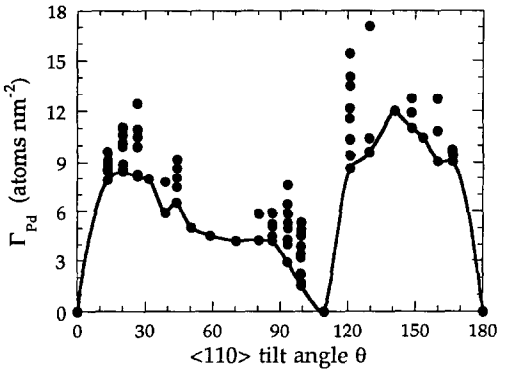

Fig. 4. The interfacial excess of Pd vs the tilt angle (θ) for the 23 ⟨110⟩ symmetric tilt GBs in Ni–4 at.% Pd at 800 K. The curve is drawn through the lowest Γ_{Pd} for each GB. The columns of points are the different Γ_{Pd} values for the multiple structures of some GBs.

GBs. The columns of points at some values of θ in Fig. 4 are the different Γ_{Pd} values for GBs with multiple structures. In some GBs the range of Γ_{Pd} values is quite large. The three structures of the $\Sigma = 11/(332)/129.52^\circ$ GB have Γ_{Pd} values ranging from 9.60 to 17.04 atoms/nm^2, while the range of Γ_{Pd} values covered by the fifteen structures of the $\Sigma = 43/(556)/99.37^\circ$ GB is 1.50–5.34 atoms/nm^{-2}. Thus, Γ_{solute} can be strongly dependent on the RBT vector and local atomic relaxations that produce different GB structures in addition to the macroscopic DOF required to characterize each GB. This illustrates another problem with using θ or any geometric parameter to predict segregation: they do not predict variations in Γ_{solute} for different structures of a single GB since they are functions of only the macroscopic geometric DOF.

3.2. *Solute distributions*

Segregation in the Ni(Pd) system is solely substitutional; Pd atoms replace Ni atoms at atomic sites in the pure Ni GB structures. While there is typically a small amount of relaxation in the atomic positions during segregation, in nearly all cases the GB structures are essentially unchanged. With the standard MC simulations of GB segregation, the average concentration of solute at each atomic site is measured. While the term segregation is generally used to indicate an enhanced solute concentration, depletion is also possible and has been observed in several cases [14]. In the remainder of this paper, however, the term segregation is used to indicate an enhancement of solute unless noted otherwise.

The distribution of solute atoms is quite different for each of the $\langle 110 \rangle$ symmetric tilt GB structures. Three examples are presented to illustrate the range of different solute distributions found. The first example is for the singular $\Sigma = 11/(113)/50.48^\circ$ GB which has the very simple solute distribution shown in Fig. 5(a). The average solute concentration at each site in this GB structure is indicated by a gray scale; the darker grays indicate higher concentrations of Pd. This data is presented in a more quantitative manner in the segregation profile normal to the boundary plane shown in Fig. 5(b). The solute concentration is highest at the boundary plane and drops to the bulk value within 0.3 nm to either side. The sites that exhibit the strongest enhancement of solute are in the GB core region formed by the overlapping GB dislocation cores. There is very little segregation outside of this core region.

The solute distributions for the remainder of the GB structures examined, however, are considerably more complex. A more typical solute distribution is the one at the $\Sigma = 33/(441)/159.95^\circ$ GB shown in Fig. 6. This solute distribution is very inhomogeneous, both in the plane of the boundary and perpendicular to it. Similar to the previous example, the highest solute concentrations are found at some of the core sites, but now there is also significant segregation outside the core region at elastically strained sites. In addition to the sites with enhanced solute concentrations, there are many sites at the boundary with low solute concentrations (shown in white), even less than the bulk concentration in some cases. Note well that even though Γ_{solute} is positive there can still be sites that are depleted of solute.

The core sites typically have the highest concentrations of solute since these sites differ the most from bulk sites. The different volumes of these sites can be energetically favorable for over- or undersized atoms; this is expected to be the most important factor for segregation in the Ni(Pd) system. Core sites can also have different atomic coordinations or neighbor geometries that are energetically favorable for solute atoms in some systems [30]. The elastically strained sites are atomic sites where the local structure is the same as that of the bulk crystal except for elastic deformations due to the GB strain field. Solute atoms interact with the GB strain fields because of their different sizes and/or elastic moduli [20]. Although segregation is generally weaker at elastically strained sites than core sites, there can be a larger number of these sites if the GB structure has long-range strain fields. Due to large strain fields in the $\Sigma = 33/(441)/159.95^\circ$ GB, the solute distribution extends to about 0.7 nm to either side of the boundary.

The $\Sigma = 33/(225)/58.99^\circ$ GB exhibits extensive segregation to both core and elastically strained sites. This GB has dissociated by emitting Shockley partial dislocations which form stacking faults as discussed in Refs [6] and [7]. The solute distribution for this GB is shown in Fig. 7. The segregation at the original boundary between -0.3 and 0.3 nm is primarily at core sites. Except for the two sites at the core of the Shockley partial dislocation, the segregation between 0.3 and 2.0 nm is entirely at elastically strained sites. The dissociation by the emission of stacking faults has created a large strain field in this structure. The sites above the partial dislocation that are under compression are depleted of the oversized Pd atoms (white sites), while the sites under tensile stress below the partial dislocation have enhanced Pd concentrations (darker sites). The two regions are separated by the (111) slip plane of the dislocation. On the left side of the partial dislocation there is an intrinsic stacking fault on the slip plane. The segregation at the stacking fault is due to the elastic strain field of the partial dislocation and not the stacking fault itself. Although segregation to stacking faults—classically called Suzuki segregation [31]—occurs in some materials [32], in an MC simulation of an isolated stacking fault in Ni–4 at.% Pd no segregation was found. A similar result is found in studies of segregation to an isolated $(a_o/2)[110]$ edge dislocation in Ni–10 at.% Cu [33]. The dislocation dissociates into two Shockley partial dislocations connected by a ribbon of stacking fault. The solute distributions around the partial dislocations are in good agreement with the distribution on the right half of Fig. 7. No

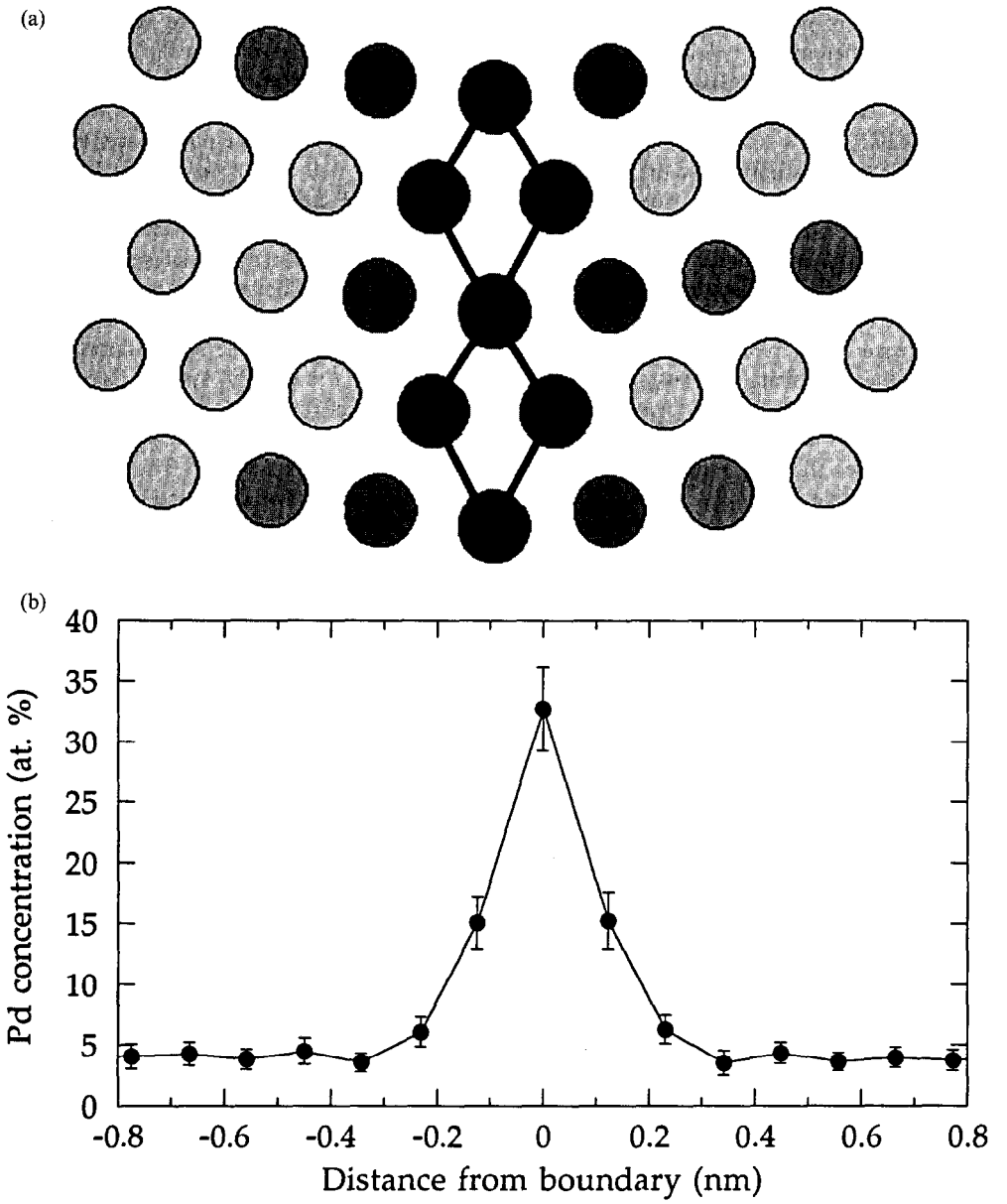

Fig. 5. Solute distribution at the $\Sigma = 11/(113)/50.48°$ GB. Darker grays indicate higher Pd concentrations in (a).

significant additional segregation to the stacking fault was detected.

3.3. *Segregation-induced structural changes*

In addition to simply substituting into sites in the structure of the GB in the pure metal, the segregation of solute atoms can also change the GB structure. While nearly all the structures investigated remained essentially unchanged, one case of a segregation-induced GB phase transition is found for the $\Sigma = 9/(221)/141.06°$ GB. In pure Ni, the structure shown in Fig. 8(a) has the lowest GB energy at both 0 and 800 K. The one higher energy structure that was found for this GB, shown in Fig. 8(b), is not stable at the higher temperature. The situation is reversed, however, because of segregation when there is a bulk concentration of 4 at.% Pd; the structure in Fig. 8(b) is stable while the structure in Fig. 8(a) is not stable. These two structures are related by an RBT of $(a_o\sqrt{2}/4)$ along the tilt axis. The RBT exchanges the (220) planes (white and black atoms) on the right-hand side of the boundary. The exact bulk concentration required to produce this phase transition was not determined. This is a congruent phase transition since the five macroscopic DOF of the GB remain unchanged [8]. Several other examples of congruent phase transitions have been reported. Simulations of congruent phase transitions have been reported for a $\Sigma = 5/(002)$ twist GB in the Pt(Ni) system [34] and for GBs in the Fe(P) system [35]. A

few additional examples of segregation-induced changes in GB structure have also been observed experimentally. The dislocation structures of twist GBs in Fe were observed to change upon segregation of Au [36], Sb [37], or S [38] to the boundaries. In MgO, segregation of Fe results in GB dissociation [39] and in Cu, segregation of Bi can cause a reversible GB faceting transition [40] where $\Sigma = 3/$ (111) facets containing an ordered Cu–Bi layer are formed [41].

3.4. *Segregation free energies*

Early studies of GB segregation employed molecular statics simulations to calculate segregation internal energies, ΔE^{seg} [42]. Because entropy is not included, ΔE^{seg} is strictly only valid at 0 K. Since the

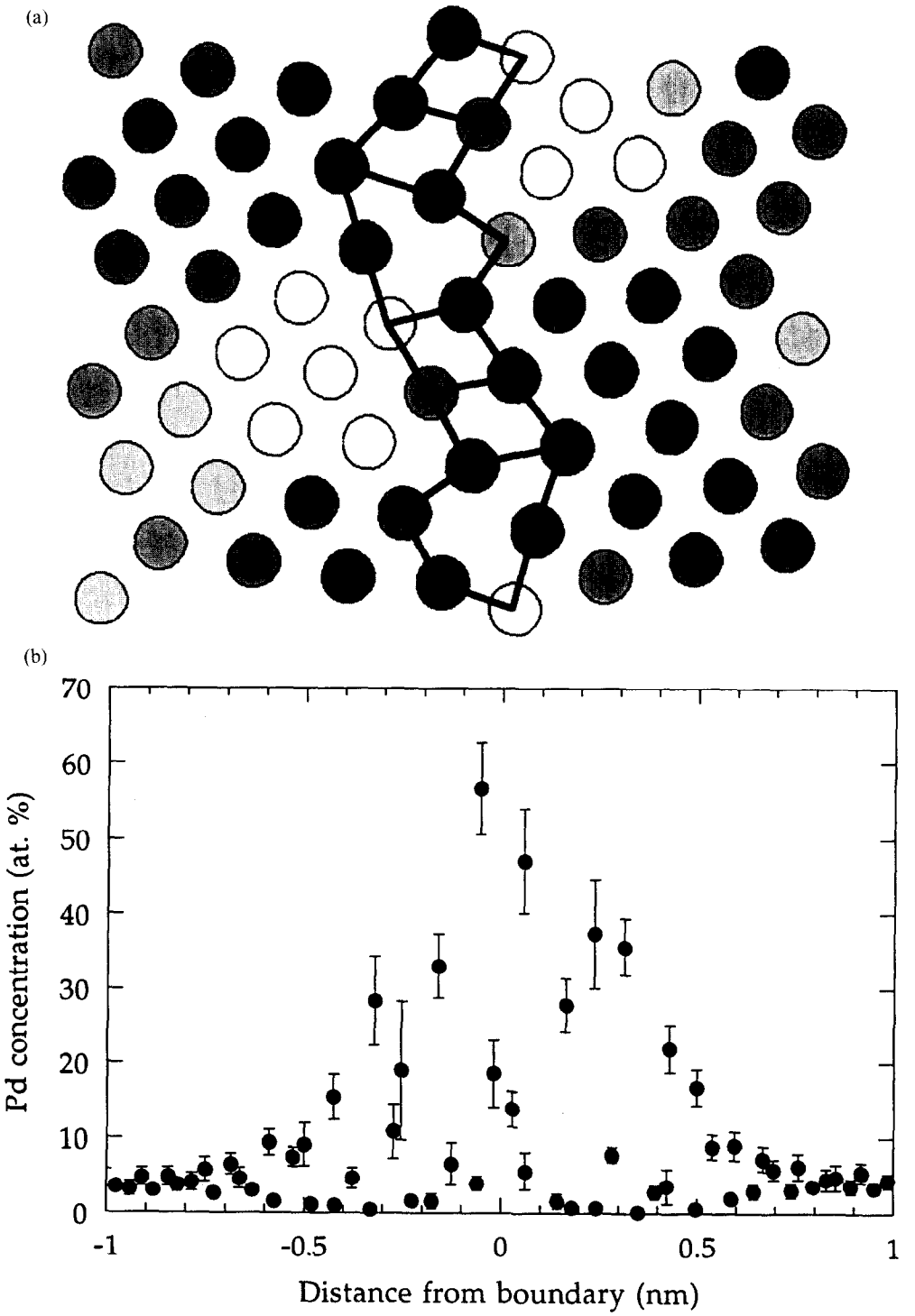

Fig. 6. Solute distribution at the $\Sigma = 33/(441)/159.95°$ GB. Darker grays indicate higher Pd concentrations in (a).

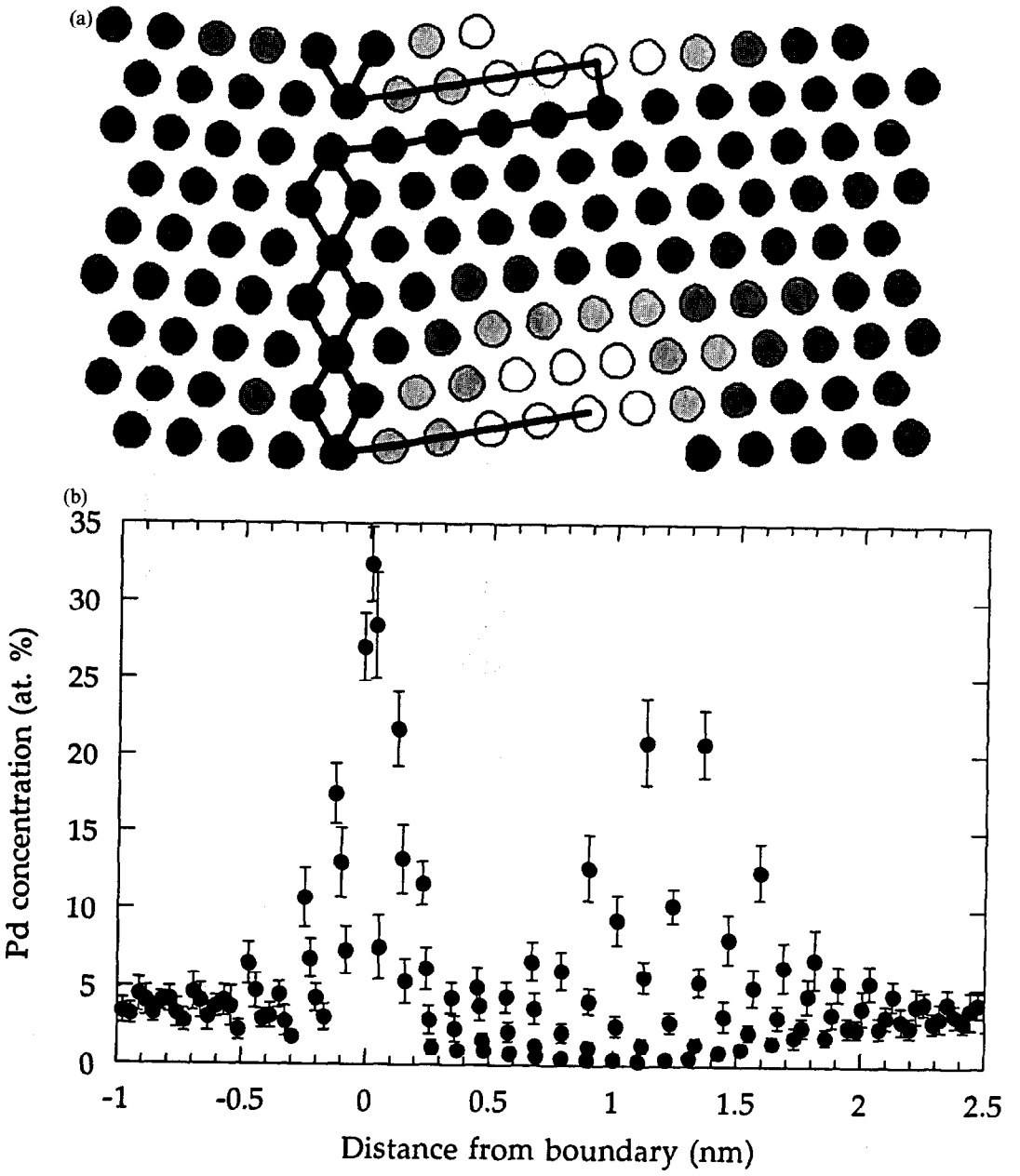

Fig. 7. Solute distribution at the $\Sigma = 33/(225)/58.99°$ GB. Darker grays indicate higher Pd concentrations in (a).

diffusion of solute atoms that is required for segregation takes place only at elevated temperatures, the segregation free energy ΔF^{seg} is the important quantity. The free energy can be either the Helmholtz or Gibbs free energy depending on whether the volume or the pressure of the system is held constant. In solid-state systems at atmospheric pressure there is generally little difference between the two free energies, so no distinction is made. Similarly, no distinction is made between the internal energy and the enthalpy. With the ODMC technique it is possible to calculate directly ΔF_i^{seg} at individual GB sites. The distribution of ΔF_i^{seg} values for the different sites in the $\Sigma = 11/(113)/50.48°$, $\Sigma = 33/(441)/159.95°$, and $\Sigma = 33/(225)/58.99°$ GB structures is plotted in Fig. 9. These plots show the range of ΔF_i^{seg} values along the x-axis and the weighting, or relative number of sites with the same ΔF_i^{seg} values, along the y-axis. Note that only a fraction of the large number of bulk crystal sites with ΔF_i^{seg} values at or near zero are included in these plots.

The ΔF_i^{seg} distribution for the $\Sigma = 11/(113)/50.48°$ GB [Fig. 9(a)] is typical of GBs with primarily core-site segregation. Segregation only occurs at a relatively small number of sites with discrete ΔF_i^{seg} values. In the $\Sigma = 11/(113)/50.48°$ GB there are only three types of sites with positive ΔF_i^{seg} values, indicating solute enhancement. The ΔF_i^{seg} distribution

of the $\Sigma = 33/(441)/159.95°$ GB [Fig. 9(b)] shows a combination of core sites and elastically strained sites. The largest ΔF_i^{seg} values are for core sites, while the broad distribution of ΔF_i^{seg} values around zero are mainly due to elastically strained sites. The negative values are for sites with solute depletion. Another example of the contribution of elastically strained sites is shown in the ΔF_i^{seg} distribution of the $\Sigma = 33/(225)/58.99°$ GB [Fig. 9(c)]. Again, the largest ΔF_i^{seg} values are for core sites but nearly all of the values below 0.1 eV, including the negative values, are for elastically strained sites. These ΔF_i^{seg} distributions demonstrate that while core sites generally have the highest values, if the GB has a long-range strain field there can be a large number of elastically strained sites.

These ΔF_i^{seg} distributions also have important implications for thermodynamic models of GB segregation. Most of these models assume that there is a single type of GB site with a single ΔF^{seg} value [25]. This is clearly incorrect even for the simplest GBs [see Fig. 9(a)]. There are a few models that do consider a distribution of ΔF_i^{seg} values for the different sites at a GB [25]. The problem with these models is how they are fit to experimental data. To reduce the number of fitting parameters, some assumption must be made about the general form of the ΔF_i^{seg} distribution. A Gaussian distribution of ΔF_i^{seg} values about some non-zero value is a typical assumption [43]. From Fig. 9 it is clear that neither this assumption nor any other that might be made will have a good fit to all the different possible ΔF_i^{seg} distributions. Thus, while thermodynamic models of GB segregation may be useful for making empirical correlations, they are not as helpful for understanding the underlying atomistic processes that cause segregation.

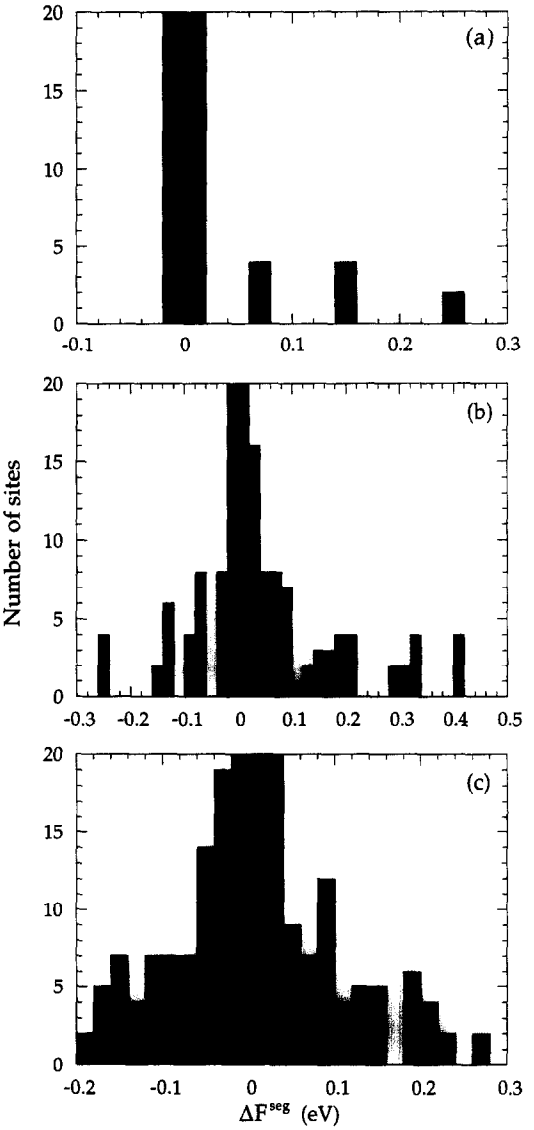

Fig. 9. Segregation free energy distributions for the (a) $\Sigma = 11/(113)/50.48°$, (b) $\Sigma = 33/(441)/159.95°$, and (c) $\Sigma = 33/(225)/58.99°$ GBs in Ni(Pd) at 800 K.

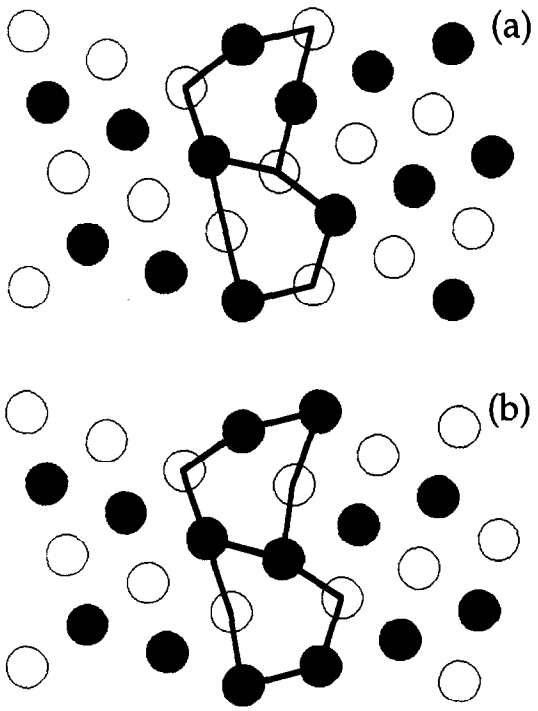

Fig. 8. Two different structures for the $\Sigma = 9/(221)/141.06°$ GB. The white and black atoms indicate the two (220) planes perpendicular to the tilt axis for this GB.

To investigate the effect of the segregation entropy ΔS^{seg}, segregation internal energies ΔE_i^{seg} for sites in several GBs have also been computed with molecular statics simulations. In most cases the ΔE_i^{seg} values overestimate the strength of the interaction between the solute and the GB compared to the ΔF_i^{seg} values. This is true for both sites with enhanced solute concentrations and sites that are depleted of solute. Thus, the ΔS_i^{seg} values must be positive for the enhanced sites and negative for the depleted sites. If

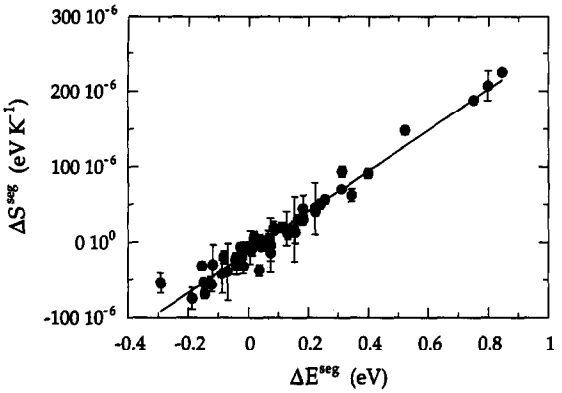

Fig. 10. Segregation entropy vs the segregation energy for multiple sites in three GBs in Ni(Pd).

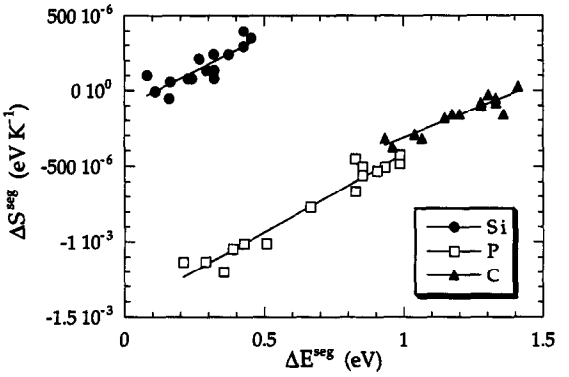

Fig. 12. Segregation entropy vs the segregation energy for Si, P and C in 15 tilt GBs in Fe–3.5 at.% Si. Data from Ref. [25].

both ΔF^{seg} and ΔE^{seg} values are known, ΔS^{seg} values can be calculated from

$$\Delta S^{seg} = \frac{1}{T}(\Delta E^{seg} - \Delta F^{seg}(T)) \qquad (7)$$

assuming that ΔE^{seg} and ΔS^{seg} are independent of temperature. An interesting relationship is observed if the ΔS^{seg} values are compared to the ΔE^{seg} values for the same GB sites. In Fig. 10, ΔS^{seg} is plotted vs ΔE^{seg} for a large number of sites in three different GB structures in Ni(Pd). There is a strong linear relationship between these values as indicated by the solid line. This relationship indicates that ΔE^{seg} values can be used to find reasonable estimates for the corresponding ΔF^{seg} values if the constants of proportionality are known. This relationship would be extremely useful if it is a general result, since it is much easier to calculate ΔE^{seg} than ΔF^{seg}.

There is some evidence that in fact this relationship is not specific to the Ni(Pd) system. Segregation entropies and energies were calculated for the Pt(Au) system at the dilute limit for several sites in the lowest energy structure of the $\Sigma = 5/(310)/53.13°$ GB [17]. There is also data from standard MC simulations of segregation to nine (002) twist GBs in the Pt–1 at.% Au system [4]. In this study the average solute concentration, C_{GB}, in a layer consisting of two (002) planes for each GB was measured over a wide range of temperatures (850–1900 K). The average ΔE^{seg} and ΔS^{seg} values for each GB were extracted from Arrhenius plots of the C_{GB} data. Both the ΔS^{seg} and ΔE^{seg} values from the individual sites in the $\Sigma = 5/(310)/53.13°$ GB and the average values from the nine (002) twist GBs are plotted in Fig. 11. Although the data for the twist GBs are only average values for the GBs and not the values at individual sites, both sets of data fall on the same line. Thus, a linear relationship is found between ΔS^{seg} and ΔE^{seg} values for both entire GBs and individual sites in GB structures in the Pt(Au) system. In another simulation study, average ΔS^{seg} and ΔE^{seg} values for a $\Sigma = 5/(002)$ twist GB over a range of temperatures and concentrations in the Ni–Cu system were calculated with the free energy minimization technique [44]. Even though these are average values for the GB, an analysis of the data reveals a linear relationship in this system as well. There is also a small amount of experimental data to support these results. The average GB concentrations of Si, P, and C have been measured over a range of temperatures for several well-characterized GBs in the Fe–3.5 at.% Si system [24]. The ΔS^{seg} and ΔE^{seg} values extracted from Arrhenius plots for 15 tilt GBs are shown in Fig. 12. Again, even though these are average values, an analysis of the data reveals a linear relationship for each of the three solutes. Correlations between internal energies and entropies have also been observed for other excess quantities such as GB energies [45] and energies of mixing in dilute solutions [46].

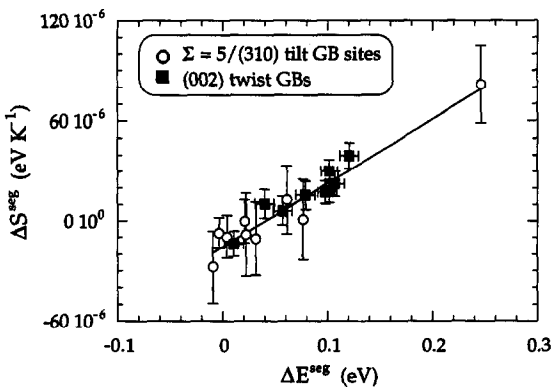

Fig. 11. Segregation entropy vs the segregation energy for several sites in the $\Sigma = 5/(310)/53.13°$ GB and average values for nine (002) twist GBs in Pt(Au). Twist GB data from Ref. [4].

4. CONCLUSIONS

In this paper, segregation of substitutional, oversized solute atoms to low stacking-fault energy f.c.c. GB structures is examined. Palladium is chosen as the solute species because it is expected to segregate strongly in the Ni matrix, primarily owing

to the 10% size misfit. The MC technique with the transmutational ensemble is employed to simulate GB segregation for a finite bulk solute concentration of 4 at.% Pd. The simulations are performed on nearly 100 different ⟨110⟩ symmetric tilt GB structures. Segregation free energies were also directly calculated for individual sites in several GB structures with the ODMC technique.

The Gibbsian interfacial excess of Pd for each GB structure is calculated from the standard MC simulations. This data is used to test various geometric GB parameters that have been used in the literature to predict how the level of segregation varies from GB to GB. Of the five parameters examined—the inverse coincident site lattice density Σ, the GB planar coincident site density, the GB average interplanar spacing, the classification level, and the tilt angle—only the tilt angle is found to have any correlation with the Gibbsian interfacial excess and the relationship is complex (Fig. 4). None of the parameters can explain the variations in the Gibbsian interfacial excess that are found in the different structures of the same GB. Thus, simple geometric parameters are insufficient for predicting GB segregation behavior because it depends intimately on the atomic scale details of the GB structures.

The equilibrium distribution of solute atoms in the GB structures is determined with standard MC simulations. Two types of segregation site are distinguished: GB core sites and elastically strained bulk sites. Since core sites deviate the most from bulk sites, the level of segregation—either enhancement or depletion of solute—is typically strongest at these sites. If, however, the GB strain fields are large, the elastically strained sites can greatly outnumber the core sites. If there is a strong elastic interaction between the solute atoms and these strain fields, segregation to elastically strained sites can be a significant component of the total segregation at these GBs. In general, the solute distribution in both core and elastically strained sites at GBs is very inhomogeneous (Figs 6 and 7). In addition to simply substituting solute atoms at sites in the GB structures of the pure material, segregation can also change the GB structure. In most cases the changes are small and the structures are not visibly different. In one GB, however, a segregation-induced congruent GB phase transition is observed (Fig. 8).

In addition to simulating solute concentrations at GBs, accurate segregation free energies at individual GB sites are calculated. The distributions of segregation free energies that were calculated for several GBs (Fig. 9) have important implications for thermodynamic models of GB segregation. Segregation internal energies, which were used in many early studies of GB segregation, are also calculated and are found to overestimate the strength of the interaction between solute atoms and the boundary compared to the segregation free energies. A strong linear relationship is found between the segregation entropies and the segregation internal energies at individual sites in the Ni(Pd) system. There is evidence from both experiments and additional simulations that this relationship holds for a number of other systems as well. These results indicate that segregation free energies can be estimated from segregation internal energies, which are much easier to calculate, if the constants of proportionality are known.

Acknowledgements—J.D.R. acknowledges the support of a Computational Sciences Graduate Fellowship program at Ames Laboratory, Ames, Iowa, the McCormick School of Engineering and Applied Sciences for a terminal year Graham Fellowship, the Alexander von Humboldt Foundation for partial support through the Max Planck Research Prize of D.N.S., and the National Energy Research Supercomputer Center for computer time. D.N.S. acknowledges support by the National Science Foundation (grant DMR-9319074, Dr B. MacDonald, grant officer). This work made use of the MRL Central Facilities at Northwestern University, which are supported by the National Science Foundation under award No. DMR-9120521. Dr D. Udler is thanked for helpful discussions.

REFERENCES

1. Hondros, E. D. and Seah, M. P., *Int. Met. Rev.*, 1977, **22,** 262.
2. Sutton, A. P. and Balluffi, R. W., *Interfaces in Crystalline Materials*. Clarendon Press, Oxford, 1995; Hondros, E. D., Seah, M. P., Hofmann, S. and Lejcek, P., in *Physical Metallurgy*, Vol. II, 4th edn, ed. R. W. Cahn and P. Haasen. North-Holland, New York, 1996, p. 1201.
3. Kuo, S.-M., Seki, A., Oh, Y. and Seidman, D. N., *Phys. Rev. Lett.*, 1990, **65,** 199; Hu, J. G. and Seidman, D. N., *Phys. Rev. Lett.*, 1990, **65,** 1615; *Scripta metall. mater.*, 1992, **27,** 693; Krakauer, B. W. and Seidman, D. N., *Rev. Sci. Instrum.*, 1992, **63,** 4071; *Phys. Rev. B*, 1993, **48,** 6724; *Mater. Sci. Forum*, 1993, **126–128,** 161; *Ibid.*, 1994, **155–156,** 393.
4. Seki, A., Seidman, D. N., Oh, Y. and Foiles, S. M., *Acta metall. mater.*, 1991, **39,** 3167; *Ibid.*, 1991, **39,** 3179.
5. Udler, D. and Seidman, D. N., *Phys. Stat. Solidi (b)*, 1992, **172,** 267; *Mater. Sci. Forum*, 1993, **126–128,** 165; *Ibid.*, 1993, **126–128,** 169; *Ibid.*, 1994, **155–156,** 189; *Acta metall. mater.*, 1994, **42,** 1959; *Interface Sci.*, 1995, **3,** 41; *J. Mater. Res.*, 1995, **10,** 1933.
6. Rittner, J. D. and Seidman, D. N., *Phys. Rev. B*, 1966, **54,** 6999.
7. Rittner, J. D., Seidman, D. N. and Merkle, K. L., *Phys. Rev. B*, 1996, **53,** R4241.
8. Cahn, J. W., *J. Phys. (Paris)*, 1982, **43,** C6-199.
9. Gibbs, J. W., *The Collected Works of J. Willard Gibbs*, Vol. 1. Yale University Press, Connecticut, 1948.
10. See for example Table 1 in Ref. [1].
11. Foiles, S. M., *Phys. Rev. B*, 1985, **32,** 7685.
12. Foiles, S. M., *Phys. Rev. B*, 1989, **40,** 11502.
13. Metropolis, N., Rosenbluth, M. N., Rosenbluth, A. W., Teller, A. H. and Teller, E., *J. Chem. Phys.*, 1953, **21,** 1087.
14. Udler, D. and Seidman, D. N., *Phys. Stat. Solidi (b)*, 1992, **172,** 267.
15. Valleau, J. P. and Torrie, G. M., in *Modern Theoretical Chemistry*, Vol. 5, ed. B. J. Berne. Plenum, New York, 1976.
16. Rittner, J. D., Foiles, S. M. and Seidman, D. N., *Phys. Rev. B*, 1994, **50,** 12004.
17. Rittner, J. D., Udler, D., Seidman, D. N. and Oh, Y., *Phys. Rev. Lett.*, 1995, **74,** 1115.

18. Foiles, S. M., Baskes, M. I. and Daw, M. S., *Phys. Rev. B*, 1986, **33,** 7983.
19. Jones, R. S., *Phys. Rev. B*, 1990, **41,** 3256.
20. Udler, D. and Seidman, D. N., *Scripta metall. mater.*, 1992, **26,** 449, 803.
21. Aust, K. T. and Rutter, J. W., *Trans. AIME*, 1959, **215,** 119; *Ibid.*, 1959, **215,** 820.
22. Palumbo, G. and Aust, K. T., *Can. Metall. Q.*, 1995, **34,** 165.
23. Hofmann, S. and Lejcek, P., *Scripta metall. mater.*, 1991, **25,** 2259.
24. Lejcek, P. and Hofmann, S., *Surf. Interface Anal.*, 1990, **16,** 546; Lejcek, P., Adamek, J. and Hofmann, S., *Surf. Sci.*, 1992, **264,** 449; Hofmann, S., Lejcek, P. and Adamek, J., *Surf. Interface Anal.*, 1992, **19,** 601; Lejcek, P., *Anal. Chim. Acta*, 1994, **297,** 165.
25. Lejcek, P. and Hofmann, S., *Crit. Rev. Solid. St. Mater. Sci.*, 1995, **20,** 1.
26. Paidar, V., *Phys. Stat. Solidi (a)*, 1985, **92,** 115.
27. Udler, D. and Seidman, D. N., *Acta metall. mater.*, 1994, **42,** 1959.
28. Hu, J. G. and Seidman, D. N., *Scripta metall. mater.*, 1992, **27,** 693.
29. Krakauer, B. W. and Seidman, D. N., *Mater. Sci. Forum*, 1993, **126–128,** 161.
30. Briant, C. L., *Metall. Trans. A*, 1990, **21,** 2339.
31. Suzuki, H., *Sci. Rep. Res. Inst. Tohoku Univ. A*, 1952, **4,** 455; *J. Phys. Soc. Jap.*, 1962, **17,** 322.
32. Herschitz, R. and Seidman, D. N., *Acta metall.*, 1985, **33,** 1547; *Ibid.*, 1985, **33,** 1565.
33. Foiles, S. M., *Mater. Res. Soc. Symp. Proc.*, 1985, **63,** 61; Smith, R. W., Najafabadi, R. and Srolovitz, D. J., *Acta metall. mater.*, 1995, **43,** 3621.
34. Udler, D. and Seidman, D. N., *Phys. Rev. Lett.*, 1996, **77,** 3379.
35. Hashimoto, M., Ishida, Y., Yamamoto, R. and Doyama, M., *Acta metall.*, 1984, **32,** 1.
36. Sickafus, K. and Sass, S. L., *Scripta metall.*, 1984, **18,** 165; *J. Vac. Sci. Technol. A*, 1985, **3,** 1525; *Acta metall.*, 1987, **35,** 69.
37. Lin, C.-H. and Sass, S. L., *Scripta metall.*, 1988, **22,** 735.
38. Lin, C.-H. and Sass, S. L., *Scripta metall.*, 1988, **22,** 1569.
39. Eastman, J. E. and Sass, S. L., *J. Am. Ceram. Soc.*, 1986, **69,** 753.
40. Donald, A., *Phil. Mag.*, 1976, **34,** 1185; Donald, A. M. and Brown, L. M., *Acta metall.*, 1979, **27,** 59; Ference, T. G. and Balluffi, R. W., *Scripta metall.*, 1988, **22,** 1929.
41. Luzzi, D. E., *Phil. Mag. Lett.*, 1991, **63,** 281; *Ultramicroscopy*, 1991, **37,** 180; Luzzi, D. E., Yan, M., Sob, M. and Vitek, V., *Phys. Rev. Lett.*, 1991, **67,** 1894.
42. Sutton, A. P. and Vitek, V., *Acta metall.*, 1982, **30,** 2011.
43. Kirchheim, R., in *Materials Interfaces*, ed. D. Wolf and S. Yip. Chapman & Hall, New York, 1992, p. 481.
44. Wang, H. Y., Najafabadi, R., Srolovitz, D. J. and LeSar, R., *Phil. Mag. A*, 1992, **65,** 625.
45. Sutton, A. P. and Balluffi, R. W., *Interfaces in Crystalline Materials*. Clarendon Press, Oxford, 1995, p. 311.
46. Lupis, C. H. P., *Chemical Thermodynamics of Materials*. North-Holland, New York, 1983, p. 461.